Fracture Resistance of Shape Memory Alloys under Thermomechanical Loading

J. Makkar[a,*], B. Young[b,*], I. Karaman[b], T. Baxevanis[a,**]

[a]*Department of Mechanical Engineering, University of Houston, Houston, TX 77204-4006, USA*
[b]*Department of Materials Science and Engineering, Texas A&M University, College Station, TX 77843, USA*

Abstract

Experimental measurements of the fracture resistance of Shape Memory Alloys (SMAs) under thermomechanical loading conditions are reported. NiTi compact tension specimens are subjected to either isothermal mechanical or isobaric thermal loading; the latter loading path is an idealization of typical loading paths that utilize these alloys as actuators. A single-parameter description of the experimental data is employed on the basis of a path-independent contour integral, which is approximated by the load–load-line displacement curves recorded from the experiments. The obtained results represent the first experimental measurement of the fracture toughness of SMAs under coupled thermo-mechanical loading, and indicate that the fracture toughness enhancement associated with crack advance under isobaric thermal loading is less pronounced than the corresponding one under isothermal mechanical loading.

Keywords: Fracture Toughness; Martensitic Phase Transformation; Shape Memory Alloys; Actuation Loading

Nomeclature

Γ	cracked configuration's bounding contour	ρ	density
		ψ	Helmholtz free energy
2γ	energy release at the crack tip per unit crack extension	Ω	cracked configuration bounded by contour Γ
δ	load-point displacement	A^{el}, A^{in}	elastic and inelastic area under load–load-line displacement curve, respectively
δ^{el}, δ^{in}	elastic and inelastic part of load-point displacement, respectively		
ε_{ij}	small-strain tensor components	A_f	austenite-finish temperature
η^{el}, γ^{el}	elastic geometry-dependent factors	A_s	austenite-start temperature
		a	crack length
η^{in}, γ^{in}	inelastic geometry-dependent factors	B	CT specimen thickness
		b	length of the unbroken ligament
σ_{cr}	critical stress required for initiation of martensitic transformation	C	unloading elastic compliance
		H	heat input
		J, J^*	path-independent contour integrals
σ_{ij}	stress tensor components		
σ_{TS}	ultimate tensile strength	J^*_{Ic}	mode-I critical J^*
σ_Y	effective yield strength	J^*_R	resistance J^*–Δa curve

*These authors have contributed equally to this letter
**Corresponding author
Email addresses: jmakkar1004@gmail.com (J. Makkar), bey1@tamu.edu (B. Young), ikaraman@tamu.edu (I. Karaman), tbaxevanis@uh.edu (T. Baxevanis)

K_{Ic}	mode-I critical stress intensity factor	T	absolute temperature
M_f	martensite-finish temperature	U	internal energy
M_s	martensite-start temperature	u	specific internal energy
n_i	unit vector normal to Γ, components of	u_i	displacement vector components
P	imposed force per unit thickness	W	CT specimen width
q_i	heat flux vector components	W_σ	density of total stress work
s	specific entropy	W_{ext}	external work done
		J^{*el}, J^{*in}	elastic and inelastic part of J^*, respectively

1. Introduction

Shape Memory Alloys (SMAs) are intermetallics, a relatively brittle class of materials, which fail predominantly by cleavage of specific crystallographic planes [1–5]. However, SMAs do display slow and stable crack extension, *i.e.*, an R-curve behavior, which is attributed mainly to phase transformation as opposed to plastic deformation in conventional ductile metals. The observed toughening (stable crack growth) is due to irreversibility effects associated with nonproportional straining in the active phase transformation zone and the shielding effect of the transformed material left in the wake of the advancing crack. Stable crack advance has been observed under nominally-isothermal mechanical loading and during cooling under a constant applied load, *i.e.*, under thermomechanical (also termed actuation) loading [6]. Crack advance under the latter loading conditions, which is characteristic to SMAs, is argued to initiate due to transformation occurring in regions in front of the crack tip, resulting in an increase of the crack driving force [7, 8].

Phase transformation (and (re)orientation of martensite variants) occurring during the fracture of SMAs call for modifications to the experimental measurement of fracture toughness standards developed for conventional structural metals [9]. Recently, Behrouz *et al.* [10] proposed a measurement of the J_R-resistance curve under nominally-isothermal mechanical loading that accounts for the mismatch among the apparent elastic properties of austenite, self-accommodated, and oriented martensite. Further modifications to the ASTM standards regarding the linear compliance method, blunting line slope, and the thickness requirement for J-dominance may be required for the standardization of fracture toughness testing for SMAs as discussed in [11].

In this technical note, a path-independent contour integral is employed for describing the driving force for crack growth in SMAs under thermomechanical (actuation) loading paths, which collapses to the J-integral under nominally-isothermal conditions. An approximation of this integral is measured experimentally from the load–load-line displacement curve recorded from experiments on NiTi Compact Tension (CT) specimen during cooling under a constant bias load. The measured R-curves are presented and compared with those obtained from the same material under nominally-isothermal conditions. The obtained results represent the first experimental measurement of the fracture toughness of SMAs under actuation loading and support the introduction of the employed contour integral as a potential unified descriptor of fracture toughness in SMAs for a wide range of thermomechanical loading conditions (and geometric configurations).

2. Material, Methodology, and Results

Fracture toughness tests were performed on $Ni_{55.7}Ti_{44.3}$ (wt%) Compact Tension (CT) specimens in an `MTS-810` servo-hydraulic test frame. The phase transition temperatures of the alloy, which was acquired from `Fort Wayne Metals` and is superelastic at room temperature (Fig. 1), are $M_f = -29°C$, $M_s = -20°C$, $A_s = -15°C$ and $A_f = 7°C$, where M_f, M_s, A_s and A_f indicate martensite finish, martensite start, austenite start and austenite finish temperatures, respectively, determined using a `TA Instruments Q2000` Differential Scanning Calorimetry (DSC). The dimensions of the specimen (schematic in Fig. 2a) were $W \approx 32.5$, $B \approx 8.5$, $0.45 \leq a/W \leq 0.55$, all in mm, where a is the crack size. The samples were cut from the bulk using wire Electrical Discharge Machining (EDM), and both sides were metallographically

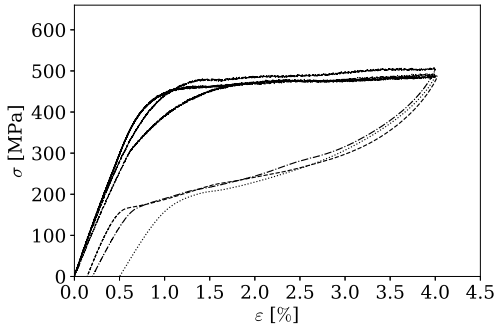

Figure 1: Uniaxial tensile loading–unloading stress–strain curves for 3 experiments performed on $Ni_{55.7}Ti$ (wt%) at room temperature.

prepared by mechanical grinding using abrasive papers to remove the EDM recast layer and for a better surface finish for optical crack size measurements. The specimens were fatigue pre-cracked in load control with load values between 0.1 and P_{max} at a frequency of 10 Hz, where P_{max}, initially set equal to 20% of the highest load value measured in the fracture experiments, was gradually decreased. During pre-cracking, the crack size was optically monitored from both sides of the specimen until the desired initial crack size (a_0) was obtained. The isothermal tests were performed in displacement control at a loading rate of 0.09 mm/min. The isobaric fracture tests were conducted by inductively heating the CT specimen to 100°C to ensure complete transformation to austenite, increasing the load to one that corresponds to 95% of isothermal K_{I_C} to ensure small-scale transformation conditions at initiation of crack growth, and then cooling down at a rate of 1°C /min to room temperature. This cooling rate was chosen to allow (i) for a homogeneous temperature throughout the sample (being slow enough), as measured using the thermocouples, and (ii) for an unloading/reloading cycle to take place in order to measure the specimen compliance at specific temperatures. Crack extension was measured by the elastic compliance method [12, 13], in accordance with the ASTM standards [9]. The compliance was measured by partial unloads and reloads, which were performed by decreasing the displacement by 0.05 mm at 0.15 mm intervals in the case of isothermal tests and by decreasing the load to 80% of the maximum load while keeping the temperature constant in the case of the isobaric tests. Load and load-line displacement (LLD) were continuously measured at a rate of 10 Hz throughout the tests using an `Interface` 2500 kN load cell and clip-on crack tip opening displacement extensometer by `Epsilon Technology Corp`. Optical images were recorded at rates of 2 fps (isothermal tests) and 0.1 fps (isobaric tests) on one side of the CT specimens, which was speckled to produce a random pattern, using a `Point Grey Blackfly` CCD camera equipped with `Canon` 18-55 mm lens at an optical resolution of 0.02 mm/pixel and were post-processed via `Vic2D-6` software (developed by `Correlated Solutions`) to measure the full-field Lagrangian strain using Digital Image Correlation (DIC) [14].

The experimental load–load-line displacement curves are shown in Figures 2. In the isothermal tests, the response is initially linear, characterized almost entirely by elastic deformation, followed by a nonlinearity associated with increasing phase transformation close to the crack tip, crack advance and resulting reorientation of martensite variants, and to a lesser extent plastic deformation [4]. The monotonicity of the applied load is interrupted by a sequence of partial unloading/reloading cycles performed in order to measure the CT specimen compliance and in turn the crack advance. The load–load-line displacement curves for the isobaric experiments are mostly linear during the application of the mechanical load at 100°C. During the subsequent cooling while the bias load is kept constant, the load-line displacement increases as the phase transformation zone expands close to the crack tip, where the stresses are high, due to the Clapeyron slope, interrupted periodically by partial unloads/reloads. Reorientation of martensite

variants is expected in the wake of the growing crack.

The experimental measurement of the path-independent contour integral J^*, introduced in Appendix A, can be based on its energetic definition

$$J^* = -\frac{d}{da}\left(\int_\Omega W_\sigma \, dV + \int_\Gamma n_i \sigma_{ij} u_j \, dS\right), \tag{1}$$

derived from (A.2) and (A.6). Under the assumption of fixed displacements (grips), the second term in the above equation vanishes, and J^* can be approximated as

$$J^* \approx \int_0^\delta \left(\frac{\partial P}{\partial a}\right)_\delta d\delta, \tag{2}$$

where P is the imposed force per unit thickness and δ is the load point displacement [15].

The J^*-value can therefore be measured from the load–load-line displacement record of the CT specimens by correlating J^* and the work of deformation $\int_0^\delta P d\delta$, *i.e.*, the area under the load–displacement curve [16–18], as $J^* = J^{*^{el}} + J^{*^{in}} = \frac{\eta^{el} A^{el}}{Bb} + \frac{\eta^{in} A^{in}}{Bb}$, where $b = W - a$ is the length of the unbroken ligament. A^{el} and A^{in} are the elastic and inelastic components of the area under the load–load-line displacement curve, respectively. η^{el} and η^{in} are geometry-dependent factors, the existence of which is discussed in [10, 11]. The expression for the J^*-integral given above is valid only for constant crack length, a. For advancing cracks, an incremental formulation is needed [19], $J_i^* = J_i^{*^{el}} + J_i^{*^{in}}$, where $J_i^{*^{el}}$ and $J_i^{*^{in}}$ are evaluated from the previous step $J_i^\alpha = \left[J_{i-1}^\alpha + \frac{\eta_{i-1}^\alpha}{B b_{i-1}} A_{i-1,i}^\alpha\right]\left[1 - \frac{\gamma_{i-1}^\alpha}{b_{i-1}}(a_i - a_{i-1})\right]$. In the last equation, the superscript $^\alpha$ stands for either ^{el} or ^{in}, $A_{i-1,i}^{el}$ and $A_{i-1,i}^{in}$ are the increments of the elastic and inelastic areas under the load–load-line displacement record from step $i-1$ to i, respectively, $A_{i-1,i}^\alpha = \frac{1}{2}(P_i + P_{i-1})(\delta_i^\alpha - \delta_{i-1}^\alpha)$, where $\delta_i^{el} = P_i C_i$ and $\delta_i^{in} = \delta_i - \delta_i^{el}$ are the elastic and inelastic components of the displacement, and C_i is the unloading elastic compliance. γ^{el} and γ^{in} are geometry-dependent factors and can be determined using η^{el} and η^{in}, respectively [10, 11].

	Isothermal		Isobaric	
Experiment	A	B	C	D
$J_{I_C}^*$-value [KJ/m^2]	31.9	30.3	27.8	24.6

Table 1: $J_{I_C}^*$-values [KJ/m^2] for $Ni_{55.7}Ti_{44.3}$ (wt%) SMA determined by the method of offset line from isothermal and isobaric fracture experiments with unloading–reloading steps to determine the system compliance.

Once J^* and Δa values are known, as outlined above and detailed in [10, 11], the J_R^*-curves are constructed according to the ASTM standards (Fig. 2). A construction line is plotted from the origin of J^* vs Δa plot with a slope of $2\sigma_Y$, where σ_Y is the effective yield strength, *i.e.*, the average of the critical stress, σ_{cr}, required for initiation of phase transformation and the ultimate tensile strength, σ_{TS}. The J^*-Δa data points that fall between two exclusion lines, which are drawn parallel to the construction line intersecting the abscissa at 0.15 mm and 1.5 mm, are plotted and a power-law regression is fit throughout. To determine the $J_{I_C}^*$ fracture toughness, an offset line is then plotted parallel to the construction line, intersecting the abscissa at 0.2 mm. The intersection of the 0.2 mm offset line and the regression line defines an interim value of the J-integral. This interim value is considered a conservative, constraint-independent fracture toughness value if the qualification requirement of ASTM standards [9], $B > 10\ J_{I_C}^*/\sigma_Y$, related to the specimen thickness is met.

The following observations can be made.

- The critical $J_{I_C}^*$-values measured using the 0.2 mm offset approach from all experiments are close to each other (Table 1). The ∼10–15% difference among the critical values measured should be

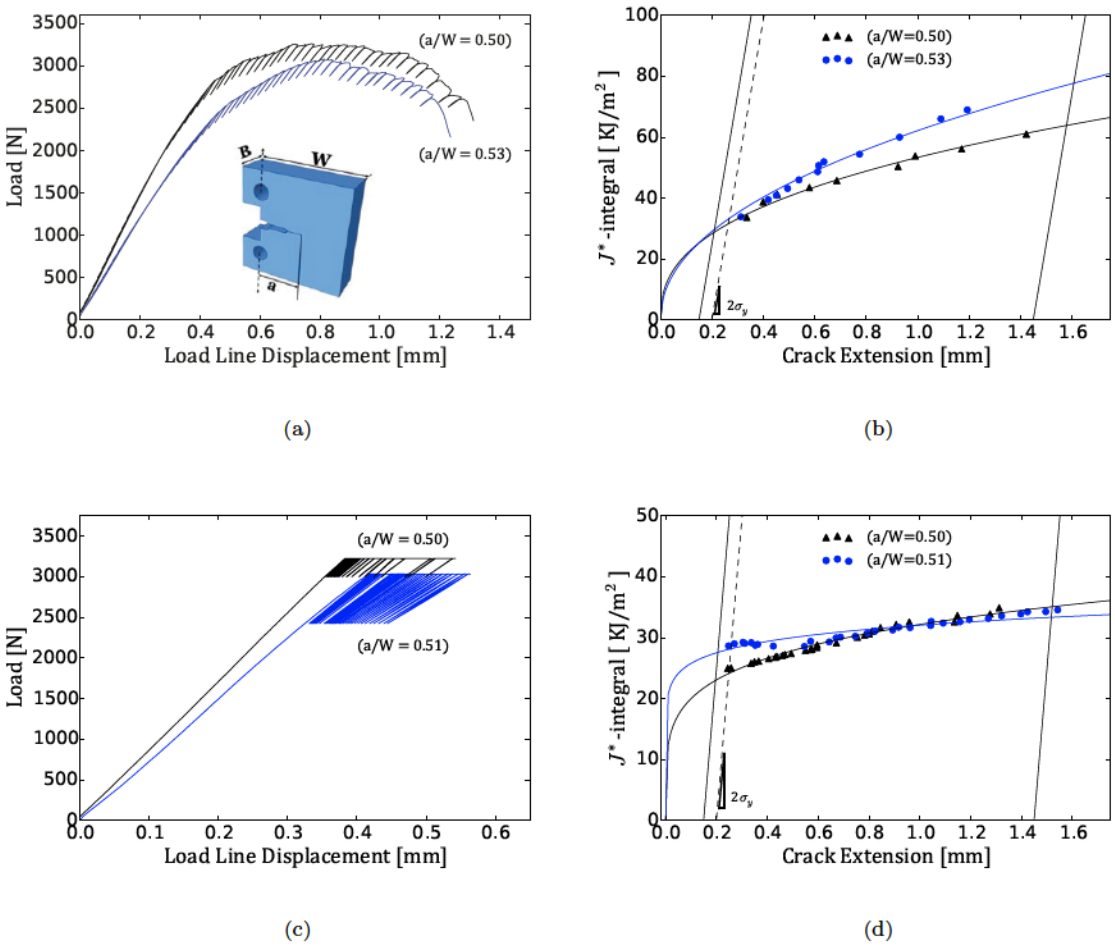

Figure 2: load–load-line displacement (LLD) and J^*_R-curves for the isobaric and isothermal fracture tests. In all experiments $0.45 < a/W < 0.55$, and $3.95 < B < 4.05$ mm. (a) & (b) isothermal experiments and (c) & (d) isobaric experiments.

attributed to the following factors: (i) The quasi-brittle transgranular (quasi-cleavage) fracture and pronounced material variability in the deformation response of SMAs (Fig. 1) result in a pronounced failure response variability; (ii) The default slope, $2\sigma_Y$, of the offset line approximates the apparent crack advance due to crack-tip blunting when there is no slow stable crack tearing. This approximation assumes that, before tearing, the crack advance is equal to one half of the crack-tip opening displacement under nominally-isothermal mechanical loading. However, crack-tip blunting in SMAs is path-dependent [20] and, thus, such a slope should assume different values for the two loading conditions (isothermal vs isobaric).

- The proximity of the critical values obtained corroborates that the path-independent J^*-integral can capture enough of the correct physics to describe with sufficient accuracy the driving force for crack advance in SMAs under both tested conditions. Due to the theoretical arguments resulting in its definition (further discussed below), the J^*-integral may be adopted as an engineering tool for fracture of SMAs under a wide range of thermomechanical loading conditions and crack configurations. It should be noted that the proximity in the $J^*_{I_C}$-values is attained while the intensity of the strain field under isothermal mechanical loading is lower than the corresponding one during

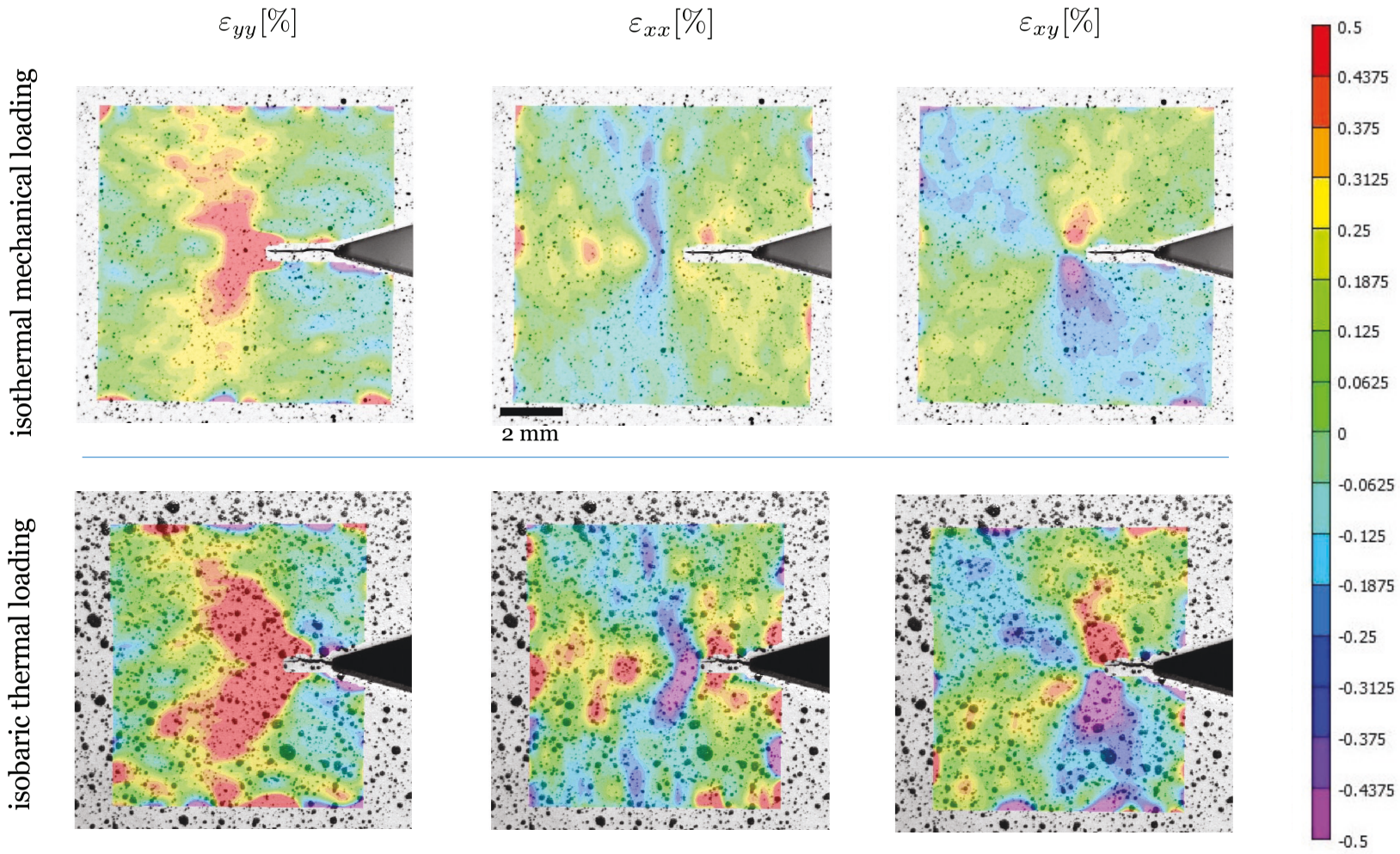

Figure 3: Surface strain contour plots obtained from *in situ* DIC on the $Ni_{55.7}Ti_{44.3}$ (wt%) CT specimens under two different thermomechanical loading paths. The y-axis is in the direction of loading. Note that the strain values at given distances from the crack tip are larger for the isobaric thermal loading although the crack length is smaller.

isobaric thermal loading (their spatial distribution being similar), which leads to the inverse conclusion regarding the intensity of stress fields (Fig. 3). In the former case, crack growth is driven by the increasing load-line displacement, which results in bias load changes at the loading pins and stress-induced martensite close to the crack tip. In the latter case, crack growth is driven by temperature changes, which result in increasing load-line displacement due to the induced phase transformation close to the crack tip while the bias load at the loading pins is kept constant.

- The slope of the isothermal J_R^*-curves is steeper than that of the isobaric ones, which indicates that the toughness enhancement associated with crack advance in the experiments under the isothermal conditions is more pronounced than the corresponding one in the experiments under the isobaric conditions. The consensus is that the toughness enhancement associated with crack advance is attributed to irreversibility effects associated with nonproportional straining in the active inelastic zone and the irrecoverable deformation left in the wake of the growing crack [21–26]. Unfortunately, it is not clear from the DIC results alone how these two stabilizing mechanisms are affected by the thermomechanical loading paths considered; numerical simulations may contribute towards the required insight. Our current assumption is that the "deterministic" toughness enhancement associated with crack advance under isothermal conditions should be independent of temperature in the temperature range that ensures a J^*-controlled crack growth (as experimentally indicated in [10] for temperatures at which the crack grows in martensite), similarly independent of load under isobaric conditions, and that these conditions are limiting cases of the general thermomechanical conditions.

Given its definition, the J^*-integral should be further applicable for thermomechanical loading paths for which the deformation response of SMAs can be approximated by a potential $\psi(\varepsilon_{ij}, T)$ such that for a given loading path there is an "1–1" correspondence between the stress $\sigma_{ij} = \rho \frac{\partial \psi}{\partial \varepsilon_{ij}}$ and strain ε_{ij}; such an approximation is expected to be valid for a wide range of thermomechanical loading paths involving nearly proportional mechanical loading and monotonic temperature changes.

3. Conclusions

A one-parameter interpretation of the experimental data from fracture experiments on SMAs under coupled thermo-mechanical loading is reported. The interpretation of the data is based on an approximation of the value of a path-independent contour integral by the load–load line displacement record measured. The obtained results, which represent the first experimental measurement of the fracture toughness of SMAs under actuation loading conditions, suggest that (i) the employed contour integral should achieve similitude for a wide range of thermomechanical loading conditions and geometric configurations, and that (ii) isothermal conditions provide a more pronounced toughness enhancement as compared to thermal loading under a constant bias load.

Acknowledgements

This study was supported by the US Air Force Office of Scientific Research under Grant No. FA9550-18-1-0276, the National Science Foundation under Grants no. CMMI-1917441 and CMMI-1917367, and by NASA-ULI under Grant No. NNX17AJ96A.

Appendix A. A path-independent contour integral for the one-parameter description of fracture toughness in SMAs under thermomechanical loading

For introducing a path-independent contour integral that can achieve similitude over a wide range of loading conditions and geometric configurations, the SMA deformation response is approximated by a thermo-hyperelastic material law with a Helmholtz free energy of the form

$$\psi(\varepsilon_{ij}, T) \equiv u\left[\varepsilon_{ij}, s(\varepsilon_{ij}, T)\right] - Ts(\varepsilon_{ij}, T), \tag{A.1}$$

where u is the specific internal energy, $s = -\frac{\partial \psi}{\partial T}$ is the specific entropy, $T = \frac{\partial u}{\partial s}$ is the absolute temperature, and ε_{ij} are the components of the small strain tensor.

Assuming quasi-static loading, the energy release at the crack tip per unit crack extension, 2γ, is given from global energy considerations as [27, 28]

$$2\gamma \dot{a} + \frac{dU}{dt} = \frac{dW_{ext}}{dt} + \frac{dH}{dt}, \tag{A.2}$$

where U is the internal energy, W_{ext} is the external work done, H is the heat input, and $\dot{a} > 0$ is the crack velocity. Assuming plane strain conditions, ignoring body forces and heat sources/sinks, and taking into account the Legendre transformation (A.1) and the definition of the small strain tensor, the above energy balance can be written

$$2\gamma \dot{a} + \frac{d}{dt}\left(\int_\Omega \rho\psi \, dV\right) = \int_\Gamma n_i \sigma_{ij} \frac{\partial u_j}{\partial t} \, dS - \frac{d}{dt}\left(\int_\Omega \rho T s \, dV\right) - \int_\Gamma q_i n_i \, dS, \tag{A.3}$$

where Ω is the cracked configuration, bounded by contour Γ, ρ is the density, σ_{ij} are the components of the stress tensor, q_i are the components of the heat flux vector, n_i those of the unit vector normal to the Γ, and u_i are the components of the displacement vector. Assuming that the displacement and temperature distributions move rigidly with the crack tip in the region Ω, the temperature is bounded at the crack tip, and the crack grows in the x_1-direction, the following relations hold true [27]

$$\frac{\partial u_j}{\partial t} = -\dot{a}\frac{\partial u_j}{\partial x_1}, \quad \frac{\partial T_j}{\partial t} = -\dot{a}\frac{\partial T_j}{\partial x_1}, \quad \frac{d}{dt}\left(\int_\Omega \rho\psi \, dV\right) = -\dot{a}\int_\Gamma n_i \rho\psi \, dS, \tag{A.4}$$

$$\int_\Gamma q_i n_i \, dS = \int_\Omega \frac{\partial q_i}{\partial x_i} \, dV = \int_\Omega \rho s \frac{\partial T}{\partial t} dV - \frac{d}{dt}\left(\int_\Omega \rho T s \, dV\right). \tag{A.5}$$

For the derivation of the last equation,

$$\frac{dU}{dt} = \frac{dW}{dt} + \frac{dH}{dt}, \tag{A.6}$$

which holds for every thermomechanical process, and (A.1) were taken into account, where $W_\sigma = \int_0^{\varepsilon_{ij}} \sigma(\varepsilon_{ij}, T) d\varepsilon_{ij}$ is density of total stress work. Given (A.4) and (A.5), the energy balance equation (A.3) takes the form

$$J^* = \int_\Gamma \left(\psi dx_2 - \sigma_{ij}\frac{\partial u_j}{\partial x_1} ds\right) + \int_\Omega s \frac{\partial T}{\partial x_1} dA = 2\gamma. \tag{A.7}$$

To prove the path-independence of J^*, it suffices to show that $J^* \equiv 0$ when integrated over any defect-free region Ω^*, bounded by contour Γ^*. To this end, note that the differential of the equation of state (A.1) asserts that

$$\frac{\partial \psi}{\partial x_k} = \frac{1}{\rho}\sigma_{ij}\frac{\partial}{\partial x_i}\left(\frac{\partial u_j}{\partial x_k}\right) - s\frac{\partial T}{\partial x_k} \overset{\frac{\partial \sigma_{ij}}{\partial x_i}=0}{\Rightarrow} \frac{\partial}{\partial x_i}\left(\rho\psi\delta_{ik} - \sigma_{ij}\frac{\partial u_j}{\partial x_k}\right) + \rho s \frac{\partial T}{\partial x_k} = 0. \tag{A.8}$$

Assuming plane strain conditions, integration of the above equation results in

$$\int_{\Gamma^*} n_i \left(\psi\delta_{ik} - \sigma_{ij}\frac{\partial u_j}{\partial x_k}\right) ds + \int_{\Omega^*} s\frac{\partial T}{\partial x_k} dA = 0, \tag{A.9}$$

and, thus, for $k = 1$, $J^* = 0$.

References

[1] T. Baxevanis and D.C. Lagoudas. Fracture Mechanics of Shape Memory Alloys: Review and Perspectives. *International Journal of Fracture*, 191(1-2):191–213, 2015.

[2] S.W. Robertson, A.R. Pelton, and R.O. Ritchie. Mechanical fatigue and fracture of nitinol. *International Materials Reviews*, 57(1):1–37, 2012.

[3] S. Gollerthan, M.L. Young, A. Baruj, J. Frenzel, W.W. Schmahl, and G. Eggeler. Fracture Mechanics and Microstructure in NiTi Shape Memory Alloys. *Acta Materialia*, 57(4):1015–1025, 2009.

[4] T. Ungár, J. Frenzel, S. Gollerthan, G. Ribárik, L. Balogh, and G. Eggeler. On the competition between the stress-induced formation of martensite and dislocation plasticity during crack propagation in pseudoelastic niti shape memory alloys. *Journal of Materials Research*, 32(23):1–10, 2017.

[5] J. Makkar and T. Baxevanis. On the fracture response of shape memory alloys by void growth and coalescence. *Mechanics of Materials*, 153:103682, 2021.

[6] S. Jape, B. Young, B. Haghgouyan, C. Hayrettin, T. Baxevanis, D.C. Lagoudas, and I. Karaman. Actuation-induced stable crack growth in near-equiatomic nickel-titanium shape memory alloys: Experimental and numerical analysis. *International Journal of Solids and Structures*, 2020. ISSN 0020-7683. doi: https://doi.org/10.1016/j.ijsolstr.2020.09.032.

[7] T. Baxevanis, A.F. Parrinello, and D.C. Lagoudas. On the Driving Force for Crack Growth During Thermal Actuation of Shape Memory Alloys. *Journal of the Mechanics and Physics of Solids*, 89: 255–271, 2016.

[8] S. Jape, T. Baxevanis, and D.C. Lagoudas. Stable crack growth during thermal actuation of shape memory alloys. *Shape Memory and Superelasticity*, 2:104–113, 2016.

[9] ASTM-E1820. Standard Test Method for Measurement of Fracture Toughness. Technical report, ASTM International, West Conshohocken, PA, 2016.

[10] B. Haghgouyan, C. Hayrettin, T. Baxevanis, I. Karaman, and D.C. Lagoudas. Fracture toughness of NiTi: Towards establishing standard test methods for phase transforming materials. *Acta Materialia*, 162:226–238, 2019.

[11] J. Makkar and T. Baxevanis. Notes on the experimental measurement of fracture toughness of shape memory alloys. *Journal of Intelligent Material Systems and Structures*, 31(3):475–483, 2020.

[12] G.A. Clarke, W.R. Andrews, P.C. Paris, and D.W. Schmidt. Single Specimen Tests for J_{Ic} Determination. In *Mechanics of Crack Growth*. ASTM International, 1976.

[13] J.A. Joyce and J.P. Gudas. Computer Interactive J_{Ic} of Testing Navy Alloys. In *Elastic-Plastic Fracture*. ASTM International, 1979.

[14] H. Schreier, J.J. Orteu, and M.A. Sutton. *Image Correlation for Shape, Motion and Deformation Measurements*. Springer US, 2009.

[15] J.R. Rice. A Path Independent Integral and the Approximate Analysis of Strain Concentration by Notches and Cracks. *Journal of Applied Mechanics*, 35(2):379–386, 1968.

[16] H. Ernst, P.C. Paris, M. Rossow, and J.W. Hutchinson. Analysis of Load-Displacement Relationship to Determine JR Curve and Tearing Instability Material Properties. In *Fracture Mechanics: Proceedings of the Eleventh National Symposium on Fracture Mechanics: Part I*. ASTM International, 1979.

[17] J.G. Merkle and H.T. Corten. J integral Analysis for the Compact Specimen, Considering Axial Force as Well as Bending Effects. Technical report, Oak Ridge National Lab., Tenn.(USA); Illinois Univ., Urbana (USA). Dept. of Theoretical and Applied Mechanics, 1973.

[18] G.A. Clarke and J.D. Landes. Evaluation of the J Integral for The Compact Specimen. *Journal of Testing and Evaluation*, 7(5):264–269, 1979.

[19] H.A. Ernst, P.C. Paris, and J.D. Landes. Estimations on J integral and Tearing Modulus T from a Single Specimen Test Record. In *Fracture Mechanics*. ASTM International, 1981.

[20] T. Baxevanis and D.C. Lagoudas. A Mode I Fracture Analysis of a Center-Cracked Infinite Shape Memory Alloy Plate Under Plane Stress. *International Journal of Fracture*, 175:1–16, 2012.

[21] J.W. Hutchinson. On steady quasi-static crack growth. Technical Report DEAP S-8, Division of Applied Sciences, Harvard University, 1974.

[22] J.R. Rice. Elastic-plastic models for stable crack growth. In *Mechanics and Mechanisms of Crack Growth (Proc. 1973)*, pages 14–39, 1975.

[23] W.J. Drugan, J.R. Rice, and T.L. Sham. Asymptotic analysis of growing plane strain tensile cracks in elastic-ideally plastic solids. *Journal of the Mechanics and Physics of Solids*, 30(6):447–473, 1982.

[24] J.R. Rice, R.M. McMeeking, D.M. Parks, and E.P. Sorensen. Recent finite element studies in plasticity and fracture mechanics. *Computer Methods in Applied Mechanics and Engineering*, 17–18: 411–442, 1979.

[25] R.H. Dean and J.W. Hutchinson. Quasi-static steady crack growth in small scale yielding. In *Fracture Mechanics*, ASTM-STP 700, pages 383–405, 1980.

[26] J. Makkar, B. Young, I. Karaman, and T. Baxevanis. Experimental observations of "reversible" transformation toughening. *Scripta Materialia*, 191:81–85, 2021.

[27] L.N. McCartney. Discussion: "the use of the j-integral in thermal stress crack problems,". *International Journal of Fracture*, 15(6):R217–R221, 1979.

[28] S.N. Atluri. Energetic approaches and path-independent integrals in fracture mechanics. In S.N. Atluri, editor, *Computational methods in the mechanics of fracture*, chapter 5, pages 121–165. North-Holland, Amsterdam, 1986.